Hindawi Publishing Corporation
EURASIP Journal on Image and Video Processing
Volume 2007, Article ID 81282, 11 pages
doi:10.1155/2007/81282

Research Article

Biomedical Image Sequence Analysis with Application to Automatic Quantitative Assessment of Facial Paralysis

Shu He,[1] John J. Soraghan,[1] and Brian F. O'Reilly[2]

[1] Department of Electronic and Electrical Engineering, University of Strathclyde, Royal College Building, Glasgow G1 1XW, UK
[2] Institute of Neurological Sciences, Southern General Hospital, 1345 Govan Road, Glasgow G51 4TF, UK

Received 26 February 2007; Revised 20 August 2007; Accepted 16 October 2007

Recommended by J.-P. Thiran

Facial paralysis is a condition causing decreased movement on one side of the face. A quantitative, objective, and reliable assessment system would be an invaluable tool for clinicians treating patients with this condition. This paper presents an approach based on the automatic analysis of patient video data. Facial feature localization and facial movement detection methods are discussed. An algorithm is presented to process the optical flow data to obtain the motion features in the relevant facial regions. Three classification methods are applied to provide quantitative evaluations of regional facial nerve function and the overall facial nerve function based on the House-Brackmann scale. Experiments show the radial basis function (RBF) neural network to have superior performance.

1. INTRODUCTION

Facial paralysis is a condition where damage to the facial nerve causes weakness of the muscles on one side of the face resulting in an inability to close the eye and dropping of the angle of the mouth. The commonest cause of facial palsy is a presumed herpes simplex viral infection, commonly referred to as Bell's palsy, which causes temporary damage to the facial nerve. Treatment of such viral infections has been the source of controversy in the past, partly because it has been difficult to audit the effectiveness of treatment. Facial paralysis may also occur as a result of malignant tumors, herpes zoster infection, middle ear bacterial infection, following head trauma, or during skull base surgical procedures, particular in the surgical removal of acoustic neuroma [1]. As the facial nerve is often damaged during the neurosurgical removal of these intracranial benign tumours of the hearing nerve, facial nerve function is a commonly used indicator of the degree of success of the surgical technique. As most methods of assessing facial function are subjective, there is a considerable variability in the results between different assessors.

Traditional assessment of facial paralysis is by the House-Brackmann (HB) grading system [2] which was proposed in 1983 and has been adopted as the North American standard for the evaluation of facial paralysis. Grading is achieved by asking the patient to perform certain movements and then using clinical observation and subjective judgment to assign a grade of palsy ranging from grade I (normal) to grade VI (no movement). The advantages of the HB grading scale are its ease of use by clinicians and that it offers a single figure description of facial function. The drawbacks are that it relies on a subjective judgment with significant inter- and intraobserver variation [3–5] and it is insensitive to regional differences of function in the different parts of the face.

Several objective facial grading systems have been reported recently. These predominantly involve the use of markers on the face [5–7]. As the color of the physical markers is a contrasting color to that of the skin, then simple threshold methods can be applied to locate the markers throughout the subjects facial movements. This makes the image processing simpler but there are negative implications as a trained technician has to accurately place the markers on the same part of the face. The success and uptake of any automatic system will hinge on the ease of use of the technology [8]. Neely et al. [9–11] and McGrenary et al. [8] measured facial paralysis by the differences between the frames of a video. Although their results correlate with the clinical HB grade, this method cannot cope with irregular or paradoxical motion in weak side. Wachtman et al. [12, 13] measured facial paralysis by examining the facial asymmetry on static images. They define the face midline by manually labeling three feature points: the inner canthus of each eye and philtrum and then measuring the intensity difference and edge difference between the two sides of the face. However, this method cannot separate the intrinsic facial asymmetry caused by facial nerve dysfunction from the extrinsic facial asymmetry caused by orientation, illumination, shadows, and the natural bilateral asymmetry.

In this paper, we present an automated, objective, and reliable facial grading system. In order to assess the degree of movement in the different regions of the face, the patient is asked to perform five separate facial movements, which are raising eyebrows, closing eyes gently, closing eyes tightly, screwing up nose, and smiling. The patient is videotaped using a front face view with a clean background. The video sequence begins with the patient at rest, followed by the five movements, going back to rest between each movement. A highly efficient face feature localization method is employed in the reference frame that is grabbed at the beginning of the video during the initial resting phase. The image of the subject is stabilized to compensate for any movement of the head by using block matching techniques. Image subtraction is then employed to identify the period of each facial movement. Optical flow is calculated to identify the direction and amount of movement between image sequences. The optical flow computation results are processed by our proposed method to measure the symmetry of the facial movements between each side of the face. These results combined with the total pixel intensity changes and an illumination compensation factor in the relevant facial regions are fed into classifiers to quantitatively estimate the degree of movement in each facial region using the normal side as the normal base line. Finally, the regional results are then fed into to another classifier to provide an overall quantitative evaluation of facial paralysis based on HB Scale. Three classification methods were applied. Experiments show the radial basis function (RBF) neural network has superior performance.

The paper is organized as follows. In Section 2, the face feature localization process is presented. In Sections 3 and 4, image stabilization and key movements detection are introduced. In Section 5, the algorithms of the extraction of motion features are developed. In Section 6, the quantitative results obtained from three classification methods are compared and Section 7 concludes the paper.

2. LOCALIZATION OF FACIAL REGIONS

Many techniques to detect faces have been developed. Yang [14, 15] classifies them into four categories: knowledge-based, feature-based, template-based, and appearance-based. Template-based and appearance-based methods can be extended to detect faces in cluttered background, different poses, and orientation. However, they need either lot of positive and negative examples to train the models or they need to be initialized manually and their computation is either time or memory intensive [15]. Our main objective is to develop an automatic assessment of facial paralysis for clinical use by measuring facial motion. In order to localize the facial features quickly, accurately and without any manual interaction, the patient is videotaped using a front face view with a clean background. Knowledge-based methods are designed mainly for face localization in uncluttered background but a method is proposed for facial feature localization. It processes a 720 × 576 image in 560 milliseconds on a 1.73 GHz laptop. It was tested using 266 images in which faces have the in-plane rotation within ±35 degrees and achieved a 95.11% accuracy for all eight facial regions as shown in Figure 1 to be localized precisely.

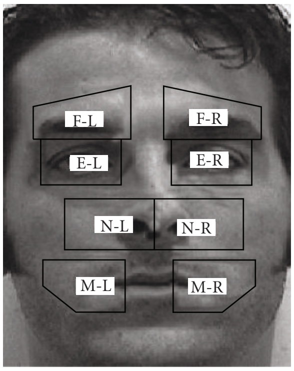

Figure 1: Illustration of facial regions. F: forehead region; E: eye region; N: nasal region; M: mouth region, L: left, R: right.

The face area is segmented, the pupils are localized and the interpupil distance is then used to scale the size of each facial region. The middle point between the two pupils is used as a fulcrum to rotate the interpupillary line to the horizontal so that the face is made perpendicular in the image. Since most subjects and especially those with a facial palsy do not have bilateral symmetrical faces, the mouth may not be symmetric on the line of the pupil middle point. The mouth corners are therefore separately localized and the middle point of the mouth is assigned. The nasal regions are initially assigned by the positions of the pupils and the middle point of mouth. They are calibrated by minimizing the difference between the left and right sides of nose. Finally, a face region map is assigned as shown in Figure 1.

2.1. Face boundary search

The face area has to be identified before starting the search for the face features. In our approach, the subject's face is viewed frontally and is the only object in the frame. The face boundary can be detected by horizontal and vertical projections of an edge-detected image. Figure 2 demonstrates that the left and right face boundaries are identified by vertical projection of a Sobel-filtered image. Similarly, horizontal projection of the binary image is used to find the top boundary of face.

2.2. Detection of the ROI of eyes and mouth

All the features of a face (eyebrows, eyes, nostril, mouth) are generally darker than the normal skin color [16] however hair may also be darker than facial features. A Gaussian filter is used to center weight the head area to remove the hair or

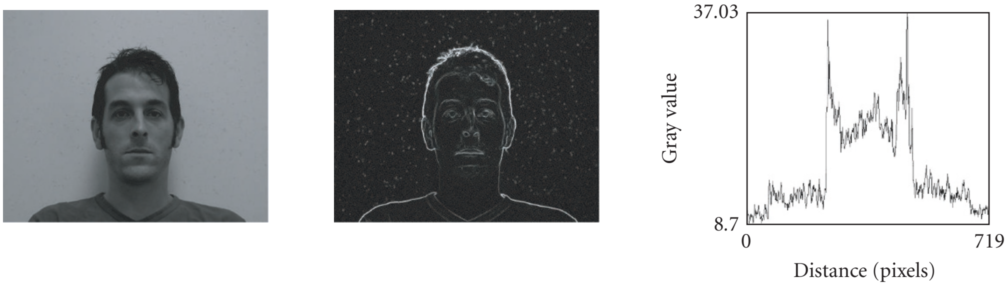

(a) Original frame

(b) Sobel filering

(c) Vertical projection

Figure 2: Face boundary detection using Sobel filter and vertical projection.

the collar. The intensity values of Gaussian-weighted image can be expressed as

$$I(x, y) = I_{\text{original}}(x, y)_* w(x, y), \tag{1}$$

where $I_{\text{original}}(x, y)$ denotes the intensity value of original image at pixel (x, y), and $w(x, y)$ is computed as

$$w(x, y) = e^{-((x-x_o)^2+(y-y_o)^2)/(2*((x_{\text{right}}-x_{\text{left}})/3)^2)}, \tag{2}$$

where x_{right} and x_{left} are the horizontal positions of right and left face boundaries. The center of the face (x_o, y_o) can be estimated as

$$\begin{aligned} x_o &= x_{\text{left}} + (x_{\text{right}} - x_{\text{left}})/2, \\ y_o &= y_{\text{top}} + (x_{\text{right}} - x_{\text{left}})_* 3/4 \end{aligned} \tag{3}$$

since the height of face is approximately 1.5 times of the width. The ROI (region of interest) of the head is assigned with the x_{right}, x_{left}, y_{top}.

Due to varied skin color and lighting conditions, a dynamic threshold is applied to the image such that only those facial features information is included for analysis. It is obtained by the solution of

$$\frac{1}{N} * \sum_{i=\text{Threshold}}^{M} C(i) = 0.1. \tag{4}$$

Here, the threshold is set to a value that only 10% of pixels present since the irises, nostrils, and the mouth border occupy no more than 10% of the ROI of head. N is the number of pixels in the ROI of head. $C(i)$ = Histogram (ROI_{head}). $M = 255$ if working on 8-bit images.

An example of an inverted, thresholded, Gaussian-weighted image is shown in Figure 3(a). The vertical position of eyebrow, eye, nostril, mouth can be determined by its horizontal projection as shown in Figure 3(b). In some cases, the eyebrow or nostril may not be identified but only the pupils and mouth corners are the essential key points necessary to assign the facial map. With the eyes and mouth vertical position and the face borders, the ROI of eyes and mouth on each side can be set to allow refining of the pupils and mouth corners positions.

2.3. Pupil search

This approach is based on the characterization of the iris and pupil. The iris-pupil region is dark compared to the white of the sclera of the eye ball and to the luminance values of the skin color. The iris localization is based on an eye template which is a filled circle surrounded by a box. The filled circle represents the iris and pupil as one part [17]. The eye width to eye height relation can be expressed as approximately 3 : 1, and the eye height is interpreted as the iris diameter [18]. Therefore, the eye template can be created as shown in Figure 4(a). This eye template is scaled automatically depending on the size of the face area. The iris is roughly localized by searching the minimum difference between the template and the ROI of the eye. The pupil is darker than the iris and therefore its position can be determined by searching the small circle with the lowest intensity value within the iris area. Here, the diameter of a small circle is set to be 1/3 of the iris diameter.

2.4. Mouth corner search

The mouth corners are detected by applying the smallest univalue segment assimilating nucleus (SUSAN) algorithm for corner extraction [19] to the ROI of the mouth. The decision whether or not a point (nucleus) is a corner is based on examining a circular neighborhood centered around the nucleus. The points from the neighborhood whose brightness is approximately the same as the brightness of the nucleus form the area referred to as univalue segment assimilating nucleus (USAN). The point (nucleus) with smallest USAN area indicates the corner. In Figure 5, the USANs are shown as grey parts and the upper left one is SUSAN. Usually, more than one point is extracted as a corner and these points are called mouth corner candidates. Three knowledge-based rules are applied to these points. First, the left corner candidates are eliminated if their horizontal distance from the middle of the pupil line is greater than 70% of the width of the search region and a similar rule is employed to the right candidates. Second, the candidates are eliminated if the horizontal distance between a left- and right-corner candidate is greater than 150% of the interpupil distance or less than 50% of the interpupil distance. Third, among the remaining left candidates, the one located furthest to the left is considered to be the left mouth corner and a similar rule is employed to

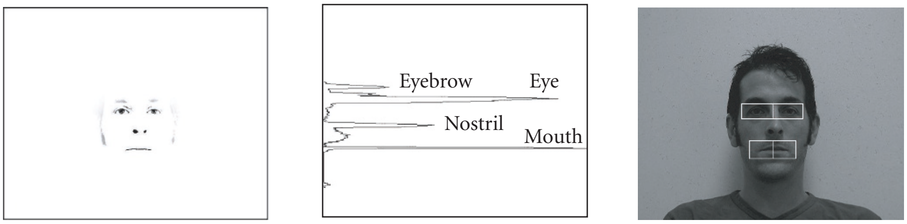

(a) Gaussian filtering of face (b) Horizontal projection (c) ROI of eyes and mouth

Figure 3: Detection of the vertical position of facial features.

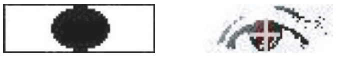

(a) Eye template (b) Detected pupil center

Figure 4: Pupil center detection.

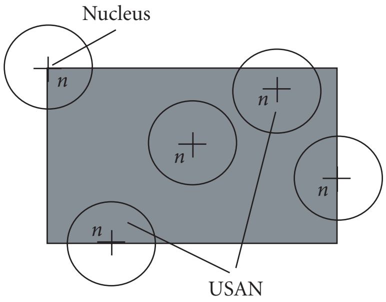

Figure 5: USAN corner detector.

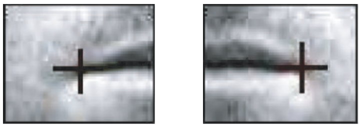

(a) (b)

Figure 6: The detected mouth corners.

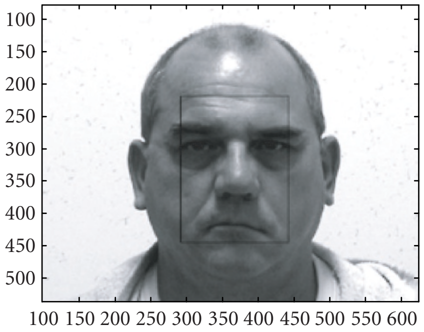

Figure 7: The ROI of the face in the reference frame.

the right candidates [20]. An example of the detected mouth corners is shown in Figure 6.

3. IMAGE STABILIZATION

Subjects will raise their head spontaneously when asked to raise there eyebrows and also shake their head while smiling. Before measuring facial motion, these rigid global motions need to be removed so that only the nonrigid facial expressions are kept in the image sequences for analysis. Feature tracking is normally considered to help solve this problem. A set of features are tracked through the image sequence and their motion is used to estimate the stabilizing warping [21]. However, in our work there are no key features in the face which do not change in structure when the movements are carried out. Therefore, all facial features are used for tracking. An ROI of the face encompassing the eyebrows, eyes, nose, and mouth in the reference frame is defined by the position of the pupils, mouth corners, and interpupils distance, as shown Figure 7. The image is stabilized by finding the best matched ROI of the face between the reference and the subsequent frames. The affine transformation given by (5) is performed on the subsequent frame. Image stabilization can be formulated as a minimization problem given by (6),

$$\begin{bmatrix} x \\ y \end{bmatrix} = \begin{bmatrix} \cos\theta & -\sin\theta \\ \sin\theta & \cos\theta \end{bmatrix} \begin{bmatrix} x' \\ y' \end{bmatrix} + \begin{bmatrix} dx \\ dy \end{bmatrix}. \tag{5}$$

Here, (x', y') is the original image coordinates, which is mapped to the new image at (x, y). dx, dy are the horizontal and vertical displacements. θ is the rotation angle. The scaling factor is not included as the distance between the subject and the camera is fixed and the face maintains constant size through images sequences in our application,

$$(dx_n{}^*, dy_n{}^*, \theta_n{}^*) = \underset{dx,dy,\theta}{\arg\min} \sum \sum_{(x,y)\subset \mathrm{ROI}} \left| T_n(x, y) - I_{\mathrm{ref}}(x, y) \right|. \tag{6}$$

Here, $dx_n{}^*, dy_n{}^*, \theta_n{}^*$ are the optimal transformation parameters for the frame n. $I_{\mathrm{ref}}(x, y)$ is the intensity of pixel at (x, y) in reference frame. $T_n(x, y)$ is the intensity of pixel at (x, y) in the warped frame n. ROI denotes the ROI of face.

dx_n, dy_n, θ_n are initialized to the optimal values in the last frame $dx_{n-1}{}^*, dy_{n-1}{}^*, \theta_{n-1}{}^*$.

4. KEY MOVEMENTS DETECTION

To examine the five key movements in the relevant regions, the timings of the five movements are identified. An algorithm based on image subtraction is proposed to determine the start and end of each movement so that information is only extracted from the appropriate time in the videos and from the appropriate facial region. The video sequence begins with the subject at rest followed by the five key movements and going back to rest in-between each movement. Therefore, the rest frames between movements have to be detected as splice points. This is achieved by totaling up several smoothed and varying thresholded pixel changes until five peaks and four valleys of sufficient separation can be extracted. The equation to produce the line from which the splice points can be detected is given in (7) as follows:

$$Y(n) = \text{smooth}\sum_{m=0}^{4}\sum_{(x,y)\subset \text{ROI}}\sum \text{thresh} \times \left(\left|I_n(x,y) - I_{\text{ref}}(x,y)\right|, (0.1 + 0.02m)\right). \quad (7)$$

Here, $I_n(x,y)$ and $I_{\text{ref}}(x,y)$ are the intensity of pixel (x,y) at the nth frame and the reference frame. The ROI is the face region, defined in session III. m is index for the threshold level. 0.1 is an empirical threshold bias to keep the high-intensity changes and remove the small pixel changes which may be produced by noise. The varying intensity of motion can be detected by changing m. By summing the different intensities of motions, the peak of motion is obvious and the splice points are easy to detect.

An example of $Y(n)$ is the highest curve in Figure 8 while the rest five curves from up to bottom are the plots at $m = 0$ to 4, respectively. The splice points are shown as the dotted lines in Figure 8. The five displacement peaks of movement correspond to the five key movements in the exercise: raising eyebrows, closing eyes gently, closing eyes tightly, scrunching nose, big smile.

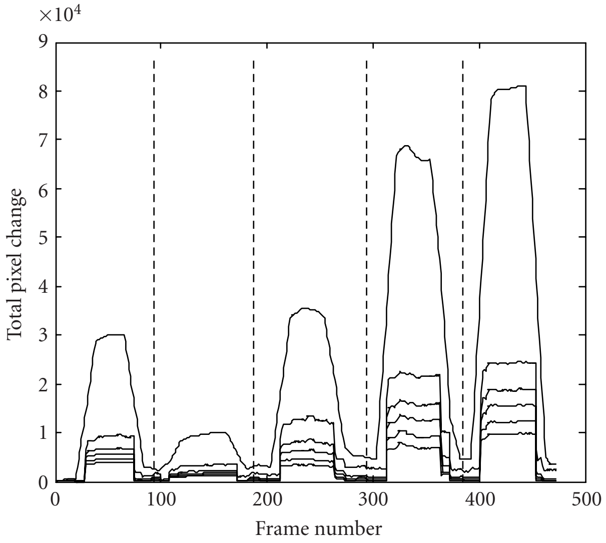

FIGURE 8: Total of thresholded, smoothed, pixel displacements.

5. REGIONAL FACIAL MOVEMENT ANALYSIS

5.1. Motion magnitude by image subtraction

Neely et al. showed that image subtraction is a viable method of quantifying facial paralysis [9, 10]. This method is therefore used to measure the motion magnitude of each key movement in the relevant region. Figure 9(a) shows a reference frame grabbed with the subject at rest. Figure 9(b) shows the frame with the subject raising eyebrows. Figure 9(c) is the difference image between Figures 9(a) and 9(b). The pixel is bright if there have been pixel changes and it is black if there has been no change. From Figure 9(c) it is clear that there are some changes in the forehead with no difference in the areas of the nose or mouth.

It has been observed that in general the more light falls on a region of the face, the more changes will be detected and the results of video taken in nonhomogeneous lighting conditions may be skewed. In our work, after the facial map is defined in the reference frame, the ratios of the intensity mean values between left side and right side in the relevant regions are calculated and then used as illumination compensation factors to adjust subsequent frames. Figure 9 illustrates a frame taken in nonhomogeneous lighting conditions. The original image lighting conditions are shown in Figure 9(a). This subject has almost completely recovered except for a mild weakness of the eye and mouth on the right side. Figure 9(c) shows difference between images Figures 9(a) and 9(b). Note that the left side of the image is the subject's right side. Here, it is obvious that more changes are detected on the left side of the forehead than on the right side. Figure 9(d) shows that the difference between images after the illumination compensation for the forehead region has been applied. The highlighted areas have the similar intensity, that is similar movement magnitude. The movement magnitude in the relevant region can be computed by (8) as

$$\text{mag}(n) = \sum_{(x,y)\subset R}\sum \left|I_n(x,y) - I_{\text{ref}}(x,y)\right|_* w(x,y)_* \text{lum}, \quad (8)$$

where w is the Gaussian weights, similar to (1), but set (x_o, y_o) to be the center of the region, x_{right} and x_{left} are right and left boundaries of the region, and lum is the illumination compensation factor, which is set to

$$\text{lum} = \sum_{(x,y)\subset \text{left}}\sum I_{\text{ref}}(x,y) / \sum_{(x,y)\subset \text{right}}\sum I_{\text{ref}}(x,y) \quad (9)$$

for right side, and lum = 1 for left side.

The graphs shown in Figure 9(e) demonstrate the full displacement results for an almost recovered subject with mild weakness at the right side of the eye and mouth. Five

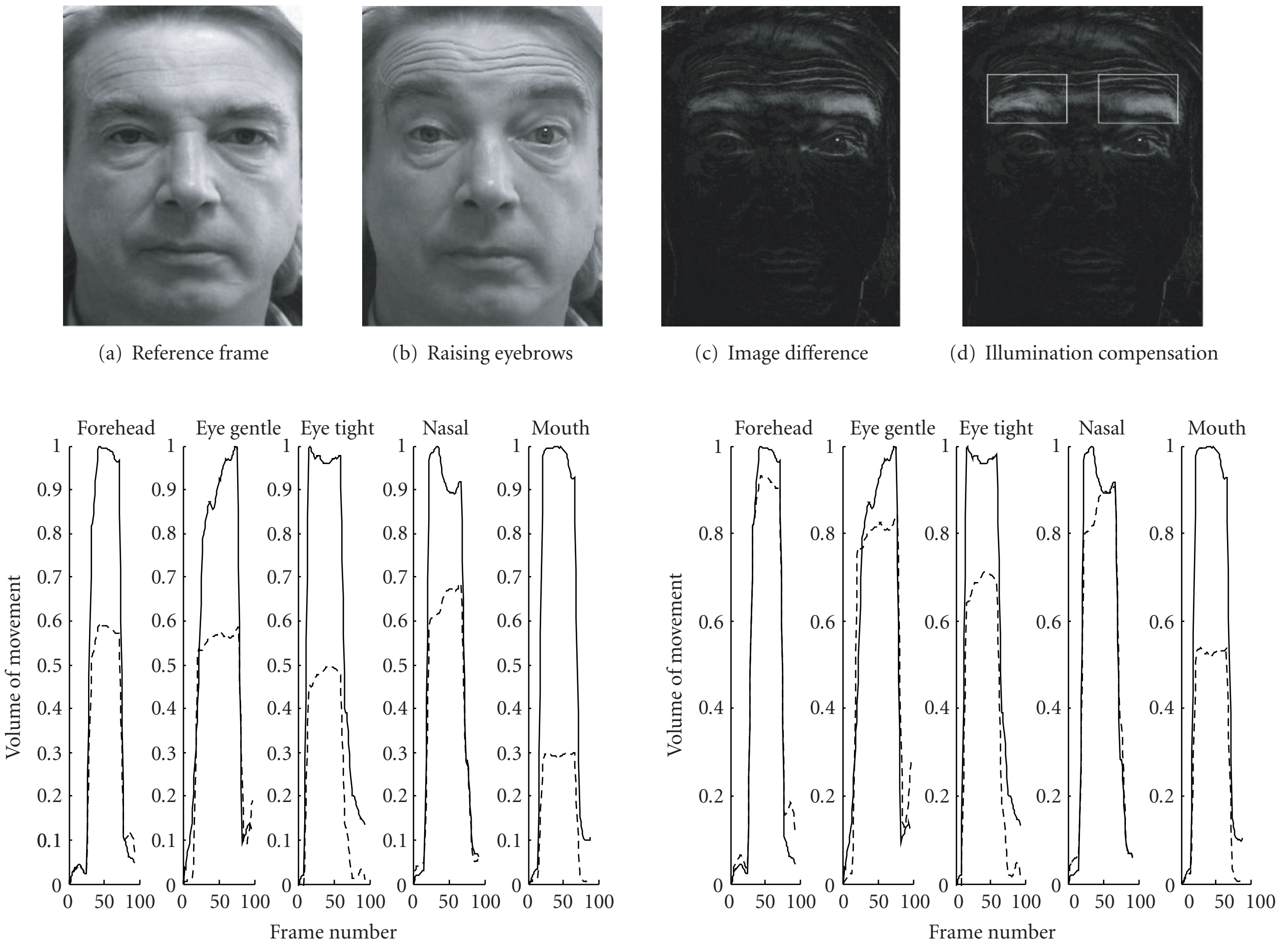

(a) Reference frame (b) Raising eyebrows (c) Image difference (d) Illumination compensation

(e) Without illumination compensation (f) With illumination compensation

Figure 9: Illustration of the solution of varying illumination.

plots in Figure 9(e) show the magnitude of the five movements in the relevant facial region. The broken line indicates the detected movement on the subject's right side of the face and the solid line indicates the movement detected on the left. The x-axis shows the frame count for each movement and the y-axis indicates the proportional volume of movement from the reference frame, the normal side being standardized to 1. The output from the forehead and nose show similar responses for the left and right sides but the movement amplitude for the eye and mouth region for right side is weaker than left side.

Figures 9(e) and 9(f) compare the results with and without illumination compensation. Figure 9(e) indicates that detected motion on the right is significantly less than the left while Figure 9(f) shows similar movement magnitude for both sides except for the eye and mouth, which is in keeping with the clinical situation.

The illumination compensation factors, which are the ratios of the intensity mean values between the left and right side for each region, are between 0.56 and 1.8 for all the subjects' videos in our study. This illumination compensation method is very effective in correcting the magnitude but it needs to be investigated further whether the illumination compensation factors can be used linearly to adjust the intensity for those videos with ratios out of this range.

5.2. Motion measurement by optical flow

The magnitude of the movement on each side of the face (i.e., Figure 9(f)) is a very effective way to compare the motion intensity between the normal and the weak sides of the face. However, it does not take into account the direction of motion. For a normal subject, the amount of motion in the relative directions on each side of the face is similar. As shown in Figure 10(e), for a normal subject producing a smile, the amount of motion in the up-left direction on the left side of the image is close to the amount in the up-right direction on the right side of the image. Figure 10(e) shows a left-palsy subject asked to smile. Although the left side has a severe paralysis, motion on the left side of the mouth is detected as the left side is drawn to the right by the movement of the right. Therefore, not only should the motion intensity be measured but the direction should also be taken into account when assessing the degree of palsy.

Optical flow is an approximation of the velocity field related to each of the pixels in an image sequence. Such a displacement field results from the apparent motion of the image brightness in time [22]. In a highly textured region, it is easy to determine optical flow and the computation converges very fast because there are high gradients in many directions at every location. Optical flow to track facial motion is advantageous because facial features and skin have a great deal of texture. There are many methods for the estimation of optical flow. Barron and Fleet [23] classify optical flow algorithms by their signal-extraction stage. This provides four groups: differential techniques, energy-based methods, phase-based techniques, and region-based matching. They compared several different methods and concluded that the Lucas-Kanade algorithm is the most accurate.

The Lucas-Kanade algorithm [24], including the pyramid approach, is employed to compute optical flow on five pairs of images, that is the reference frame and the frame with maximum motion in each movement. Using the pyramid method with reduced resolution allows us to track the large motion while maintaining its sensitivity to subtle facial motion and allows the flow computation to converge quickly. Figures 10–12 show the results of optical flow estimation for a normal subject, a left-palsy subject and a right-palsy subject. In Figure 10, the motion flows are approximately symmetrical between two highlighted regions. There is almost no motion in the left side of the forehead and the nose in Figures 11(a) and 11(d), whereas there is an obvious flow towards right on the left side of mouth in Figure 11(e). Note that the right side of image is the subject's left side. Figure 12 shows a subject who cannot close his eye but when attempting to do so his iris moves upward. Although this movement of the iris is detected by the image subtraction method, it should be discriminated from the motion of the eyes closing and removed from the calculation of the degree of movement. Figures 12(b) and 12(c) shows little flow detected in the right eye confirming the severe palsy in the eye region.

In each facial feature region, the flow magnitude is thresholded to reduce the effect of small computed motions which may be either produced from textureless areas or affected by illumination and the flow magnitude is center weighted by a Gaussian filter. Given the thresholded flow vector $\vec{v_i} = (u_i, v_i)$ in the region, the overall flow vector of each region can be expressed as $\vec{v} = (u, v)$, the components of the vector, u and v, denote of overall displacement on the horizontal and vertical direction. $u = \sum_i u_{i*}w_i$, $v = \sum_i v_{i*}w_i$, here w_i is the Gaussian weights, similar to (1), but set (x_o, y_o) to be the center of the region, x_{right} and x_{left} are right and left boundaries of the region.

When subjects raise their eyebrows, close their eyes or screw up their nose, the muscles in each relevant region move mainly in the vertical direction. Studies have shown that even for normal subjects neither the amplitude nor the orientation of horizontal displacements on each side are consistently symmetrical. Figure 13 shows two normal subjects raising their eyebrows. In Figure 13(a), the mean horizontal displacements are negative for both sides, that is, in the same direction, while in Figure 13(b), the mean horizontal displacements on each side are opposite. In Figure 13(a), the amplitude of the mean horizontal displacements in the left side is larger than that in the right side, while in Figure 13(b) they are similar. The movement in the horizontal direction does not contribute much information when measuring the symmetry of the eyebrow, eyes, or nose movements. Therefore, the displacements strength and the vertical displacements are only used for these symmetry measurements. The symmetry of the facial motion is quantified by

$$\text{Sym}_y = 1 - \frac{|v_{\text{left}} - v_{\text{right}}|}{|v_{\text{left}}| + |v_{\text{right}}|}, \tag{10}$$

$$\text{Sym}_r = 1 - \frac{\big|\|\vec{v}_{\text{left}}\| - \|\vec{v}_{\text{right}}\|\big|}{\|\vec{v}_{\text{left}}\| + \|\vec{v}_{\text{right}}\|}, \tag{11}$$

where v_{left} and v_{right} are the overall vertical displacements for left side and right side, $\vec{v}_{\text{left}}$ and $\vec{v}_{\text{right}}$ are the overall flow vector for left side and right side. Sym_y and Sym_r will be within the range 0-1. The motions on each side of face are symmetrical when both approximate 1. When both approximate 0 the dysfunctional side has no movement at all. While when $\text{Sym}_y = 0$ and $\text{Sym}_r = 1$ indicate that the motion on each side is the same amplitude but opposite direction, that is one eye closed, the other eye cannot close but the iris moves upwards in the presence of severe paralysis.

The muscle around the mouth will move to the side of face when normal people smile. The horizontal displacements should be negative, that is, move towards the left on the left side of mouth; and should be positive, that is, move towards the right on right side. This is used as a constraint to calculate the overall flow vector of left region and right region, formulated as

$$\begin{aligned}
u_{\text{left}} &= \sum_{u_i<0} u_{i*}w_i, \\
v_{\text{left}} &= \sum_{u_i<0} v_{i*}w_i, \\
u_{\text{right}} &= \sum_{u_i>0} u_{i*}w_i, \\
v_{\text{right}} &= \sum_{u_i>0}.
\end{aligned} \tag{12}$$

In the left mouth region, each motion vector with a negative horizontal displacement is taken into account. Only those with the positive horizontal displacement are taken into account for the right side. This allows elimination of the apparent muscle movement on the weak side produced by the muscles on the normal side as in Figures 11(e) and 12(e).

This method was tested in 197 videos. Sym_y and Sym_r are correlated with HB grade around 0.83 in the forehead and around 0.7 in the rest of the region. Details are shown in Table 1.

6. QUANTITATIVE ASSESSMENT AND EXPERIMENTS

6.1. Quantitative assessment

To map the motion magnitude and optical flow information into a HB grade is a classification problem.

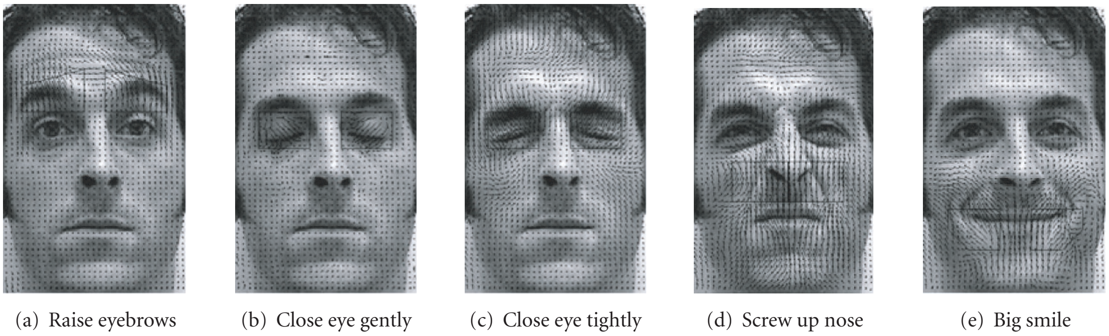

(a) Raise eyebrows (b) Close eye gently (c) Close eye tightly (d) Screw up nose (e) Big smile

Figure 10: Results of optical flow estimation on five frames with peak motion for a normal case.

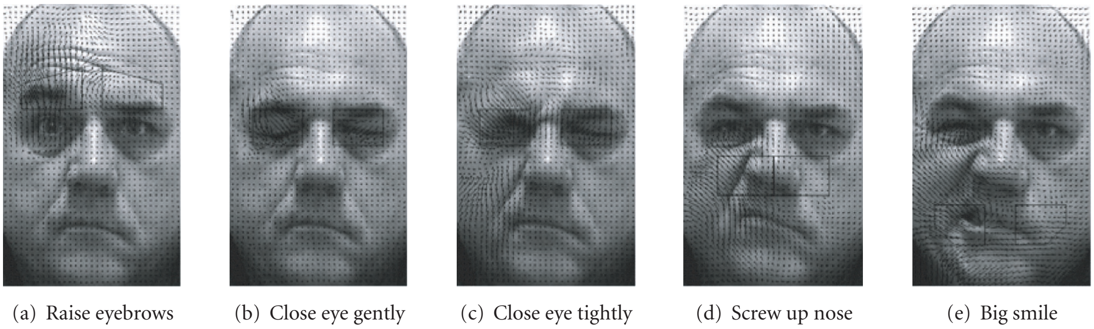

(a) Raise eyebrows (b) Close eye gently (c) Close eye tightly (d) Screw up nose (e) Big smile

Figure 11: Results of optical flow estimation on five frames with peak motion for a left palsy case.

Table 1: Correlation analysis between Sym_y, Sym_r, and HP grade.

	Corr with Sym_y	Corr with Sym_r
Forehead	0.8303	0.8381
Eye gentle	0.7351	0.7603
Eye tight	0.6968	0.7071
Nose	0.6981	0.7199
Mouth	0.7158	0.7206

There are a number of classification methods. k-nearest neighbor (k-NN), artifical neural network (ANN), and surport vector machine (SVM) are the most widely used classifiers. They can be used successfully for pattern recognition and classification on data sets with realistic sizes. These three classification methods were employed for the quantitative assessment of regional paralysis and the overall facial paralysis.

The HB grades the overall facial nerve function and it is insensitive to small changes in each facial region.

The regional facial function is measured by examining the key movements in the relevant region and classified to six grades from 1 (normal) to 6 (total paralysis). Five classifiers are trained for the five movements, respectively. Each has four inputs as follows.

(1) $\arg\min(\mathrm{mag}_{\mathrm{left}}, \mathrm{mag}_{\mathrm{right}})/\arg\max(\mathrm{mag}_{\mathrm{left}}, \mathrm{mag}_{\mathrm{right}})$. Here, $\mathrm{mag}_{\mathrm{left}}, \mathrm{mag}_{\mathrm{right}}$ denotes the total relative pixel change in the region from the resting face to the peak of the movement, which can be calculated using (8). The input value computed here gives the ratio of the total pixel change between the dysfunctional side and the normal side.

(2) The illumination compensation factor, calculated by (9), which is the ratio of mean intensities for each region between the dysfunctional side and the normal side. Although the illumination compensation factors can be used to correct the magnitude if it is between 0.56 and 1.8, the performance of this linear compensation is not ideal. As shown in Figure 9(d), the two highlighted regions have the similar intensity but are not identical. In order to further compensate for the illumination, the illumination factor is included as an input to the classifier.

(3) Sym_y, defined by (10), represents the symmetry relative to the vertical component of the total amount of displacements from the resting face to the peak of movement.

(4) Sym_r, defined by (11), represents the symmetry relative to the strength of the total amount of displacements from the resting face to the peak of movement.

Outputs are graded from 1 to 6, with 6 representing severe palsy and 1 being normal. These regional results are then used as the inputs for the overall classifier to analyze the HB overall palsy grade.

6.2. Experiments

There are 197 subject videos in our database taken from subjects with Bell's palsy, Ramsey Hunt syndrome, trauma, and

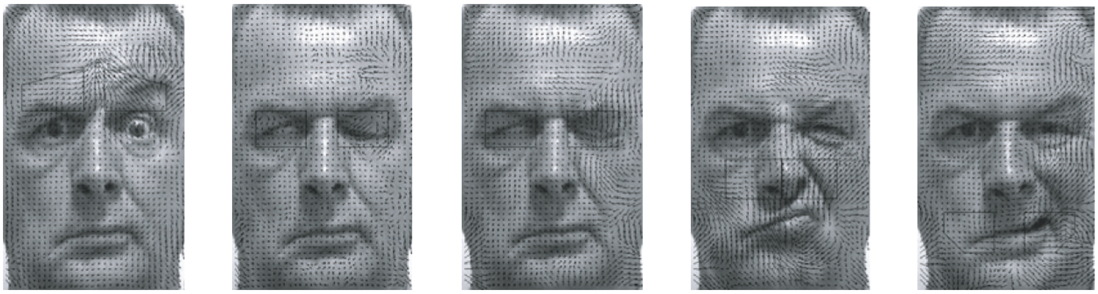

(a) Raise eyebrows (b) Close eye gently (c) Close eye tightly (d) Screw up nose (e) Big smile

Figure 12: Results of optical flow estimation on five frames with peak motion for a right palsy case.

Table 2: Test data performance of RBF NN.

Disagreement	0	1	2	3	4	5	≤ 1
Forehead	68.71	24.52	4.02	2.75	0	0	93.23
Eye gentle	44.36	47.90	3.23	4.51	0	0	92.26
Eye tight	41.27	51.84	3.69	3.20	0	0	93.11
Nose	61.78	24.53	10.18	3.51	0	0	86.31
Mouth	49.80	38.22	8.43	3.55	0	0	88.02
HB	63.92	30.26	5.82	0	0	0	94.18

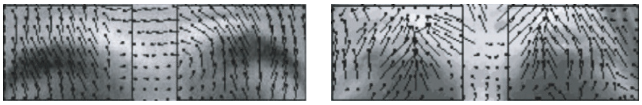

(a) Normal subject I (b) Normal subject II

Figure 13: Results of optical flow estimation on forehead for two normal subjects.

other aetiologies as well as normal subjects. Their HB and regional gradings were evaluated by a clinician. As the dataset was not large, the leave-k-out-cross-validation test scheme instead of k-fold was adopted.

Multilayer perceptron (MLP) network and radial basis function (RBF) network are the most popular neural network architectures [24, 25]. Experiments show RBF networks provide consistently better performance than MLP networks for facial palsy grading. The centers of each RBF NN were initialized using the k-means clustering algorithm before starting training.

Tables 2, 3, and 4 present the average classification performance, in percentages, for the 20 repetitions of the leave-k-out cross-validation, with k = 20. The numbers in the first columns give the percentage of the results which are the same as the clinician's assessments. Columns 2–6 show the percentages where the disagreement is from 1 to 5 grades, respectively. The last columns show the percentage of the disagreement within 1 grade. The comparison of the performance is graphically illustrated in Figure 14. The results show that the RBF NN outperforms the k-NN and SVM. The disagreement within one grade between the results of the RBF NN and the clinical assessment is 94.18% for the HB overall grading, which is 5.38% higher than SVM and 10.71% higher than k-NN. The variation of the performance for RBF NN is similar to that of SVM. Both RBF NN and SVM provide more stable results than the k-NN. The variation of the results of disagreement within 1 grade is shown in Table 5.

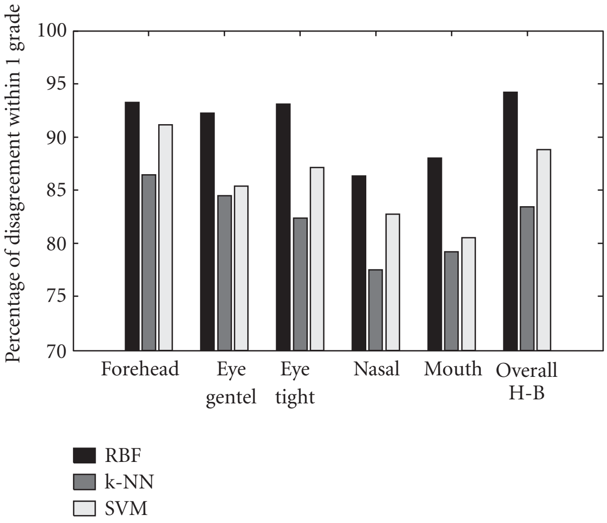

Figure 14: Comparison of the performance of three RBF, k-NN, SVM.

The RBF network has similar structure as SVM with Gaussian kernel. RBF networks are typically trained in a maximum likelihood framework by minimizing the error. SVM takes a different approach to avoid overfitting by maximizing the margin. Although SVM outperforms RBF networks from the theoretical view, they can be competitive when the dimensionality of the input space is small. There

Table 3: Test data performance of k-NN.

Disagreement	0	1	2	3	4	5	≤ 1
Forehead	65.33	21.12	5.79	4.61	3.15	0	86.45
Eye gentle	39.91	44.57	7.73	5.90	1.89	0	84.48
Eye tight	36.73	45.62	6.65	5.28	5.72	0	82.35
Nose	55.68	21.83	13.47	7.11	1.91	0	77.51
Mouth	44.01	35.19	11.62	8.35	0.83	0	79.20
HB	58.13	25.26	12.88	3.73	0	0	83.39

Table 4: Test data performance of SVM with Gaussian radial basis function kernel.

Disagreement	0	1	2	3	4	5	≤ 1
Forehead	65.98	25.14	7.22	1.66	0	0	91.12
Eye gentle	41.05	44.32	9.81	4.82	0	0	85.37
Eye tight	38.79	48.33	10.88	2.10	0	0	87.12
Nose	59.28	23.45	14.32	2.95	0	0	82.73
Mouth	43.37	37.11	17.58	1.94	0	0	80.48
H-B	59.73	29.07	11.2	0	0	0	88.80

Table 5: The variation of the performance (Disagreement ≤ 1).

	RBF	k-NN	SVM
Forehead	5.6%	8.1%	7.1%
Eye gentle	11.3%	14.6%	10.7%
Eye tight	11.0%	15.2%	10.2%
Nose	9.1%	13.5%	8.0%
Mouth	10.2%	14.2%	9.3%
HB	7.1%	13.3%	7.8%

are only 4 or 5 inputs in our work. The centers of each RBF NN were initialized using the k-means clustering algorithm before starting training. Experiments show that RBF networks can discover the nonlinear associations better than SVM and k-NN in our application.

6.3. Discussion

The most encouraging aspect of these results is that the disagreement within one grade between the results of the RBF NN and the clinical assessment was around 90% for regional grading and 94% for the HB overall grading. The best that clinical assessment alone can achieve is usually an inter- or intraobserver variation of at least one grade. The system is objective and stable as it provides the same regional results and HB grade during the analysis of different videos taken from the same subjects on the same day whereas clinicians have inconsistent assessments.

The subjects who could not finish the prescribed movements correctly failed to be correctly classified. The patients were asked to practice the prescribed facial movements before being videotaped. These practice runs help minimize the noncorrespondence error.

The results show that the best agreement is in the forehead region as in this region the optical flow can be estimated with a high degree of accuracy. The estimation of the optical flow in the eye region has poor performance, especially for those faces with makeup or very irregular wrinkles on the eyelids. The structure of the eyebrows does not change significantly during raising of the eyebrows but the structure of eyes changed significantly when performing eye closure. The error of optical flow estimation in the other regions is the major reason for their disagreement being greater than 1 grade. More effective algorithms for the optical flow estimation should be investigated to offer more reliable results and for better performance of the networks for regional measurement. The disagreements between the clinical and the estimated H-B values are greater than 1 grade only when the regional results introduce a higher average error.

The proposed algorithms have been implemented in Java with Java Media Framework (JMF) and ImageJ. The average video with 500 frames can be processed in 3 minutes on a 1.73 GHz laptop. This overall processing time should satisfy the requirement of the practicing physician.

7. CONCLUSION

We have proposed an automatic system that combines facial feature detection, face motion extraction, and facial nerve function assessment by RBF networks. The total pixel change was used to measure the magnitude of motion. The optical flow is computed and analyzed to identify the symmetry relative to strength and direction on each side of the face. RBF neural networks are applied to offer regional palsy grades and HB overall palsy grade. The results of regional evaluation in forehead and the overall HB grade are the more reliable. The errors are mainly introduced by nonstandard facial movements and the incorrect estimation of the optical flow. Therefore, encouraging patient to perform the key movements correctly and a more accurate estimation of optical flow should improve the performance of the system. The present results are encouraging in that they indicate that it should be possible to produce a reliable and objective method of measuring the degree of a facial palsy in a clinical setting.

REFERENCES

[1] C. Diamond and I. Frew, *The Facial Nerve*, Oxford University Press, Oxford, UK, 1979.

[2] J. W. House, "Facial nerve grading systems," *Laryngoscope*, vol. 93, no. 8, pp. 1056–1069, 1983.

[3] C. H. G. Beurskens and P. G. Heymans, "Positive effects of mime therapy on sequelae of facial paralysis: stiffness, lip mobility, and social and physical aspects of facial disability," *Otology & Neurotology*, vol. 24, no. 4, pp. 677–681, 2003.

[4] J. B. Kahn and R. E. Gliklich, "Validation of a patient-graded instrumnet for facial nerve paralysis: the FaCE scale," *Laryngoscope*, vol. 111, no. 3, pp. 387–398, 2001.

[5] J. Linstrom, "Objective facial motion analysis in patients with facial nerve dysfunction," *Laryngoscope*, vol. 112, no. 7, pp. 1129–1147, 2002.

[6] H. Scriba, S. J. Stoeckli, D. Veraguth, and U. Fisch, "Objective evaluation of normal facial function," *Annals of Otology, Rhinology & Laryngology*, vol. 108, no. 7, part 1, pp. 641–644, 1999.

[7] P. Dulguerov, F. Marchal, and D. Wang, "Review of objective topographic facial nerve evaluation methods," *American Journal of Otology*, vol. 20, no. 5, pp. 672–678, 1999.

[8] S. McGrenary, B. F. O'Reilly, and J. J. Soraghan, "Objective grading of facial paralysis using artificial intelligence analysis of video data," in *Proceedings of the 18th IEEE Symposium on Computer-Based Medical Systems(CBMS '05)*, pp. 587–592, Dublin, Ireland, June 2005.

[9] J. G. Neely, A. H. Joaquin, L. A. Kohn, and J. Y. Cheung, "Quantitative assessment of the variation within grades of facial paralysis," *Laryngoscope*, vol. 106, no. 4, pp. 438–442, 1996.

[10] T. D. Helling and J. G. Neely, "Validation of objective measures for facial paralysis," *Laryngoscope*, vol. 107, no. 10, pp. 1345–1349, 1997.

[11] J. G. Neely, "Advancement in the evaluation of facial function," in *Advances in Otolaryngology—Head and Neck Surgery*, vol. 15, pp. 109–134, Elsevier Science, New York, NY, USA, January 2002.

[12] G. S. Wachtman, Y. Liu, T. Zhao, et al., "Measurement of asymmetry in persons with facial paralysis," in *Proceedings of Combined Annual Conference of the Robert H. Ivy and Ohio Valley Societies of Plastic and Reconstructive Surgeons*, Pittsburgh, Pa, USA, June 2002.

[13] Y. Liu, K. L. Schmidt, J. F. Cohn, and S. Mitra, "Facial asymmetry quantification for expression invariant human identification," *Computer Vision and Image Understanding*, vol. 91, no. 1-2, pp. 138–159, 2003.

[14] M.-H. Yang, D. J. Kriegman, and N. Ahuja, "Detecting faces in images: a survey," *IEEE Transactions on Pattern Analysis and Machine Intelligence*, vol. 24, no. 1, pp. 34–58, 2002.

[15] M. H. Yang, "Recent advances in face detection," in *Proceedings of 17th International Conference on Pattern Recognition (ICPR '04)*, Cambridge, UK, August 2004.

[16] G. C. Feng and P. C. Yuen, "Multi-cues eye detection on gray intensity image," *Pattern Recognition*, vol. 34, no. 5, pp. 1033–1046, 2001.

[17] J. Rurainsky and P. Eisert, "Template-based eye and mouth detection for 3D video conferencing," in *Visual Content Processing and Representation*, vol. 2849 of *Lecture Notes in Computer Science*, pp. 23–31, Springer, Berlin, Germany, 2003.

[18] L. G. Farkas, *Anthropometry of the Head and Face*, Raven Press, New York, NY, USA, 1995.

[19] S. M. Smith and J. M. Brady, "SUSAN—a new approach to low level image processing," *International Journal of Computer Vision*, vol. 23, no. 1, pp. 45–78, 1997.

[20] M. Hess and G. Martinez, "Facial feature extraction based on the smallest univalue segment assimilating nucleus (SUSAN) algorithm," in *Proceedings of the Picture Coding Symposium (PCS '04)*, San Francisco, Calif, USA, December 2004.

[21] C. Guestrin and F. Cozman, "Image stabilisation for feature tracking and generation of stable video overlays," Tech. Rep. CMU-RI-TR-97-42, Robotics Institute, Carnegie Mellon University, Pittsburgh, Pa, USA, November 1997.

[22] M. Elad and A. Feuer, "Recursive optical flow estimation—adaptive filtering approach," in *Proceedings of the 19th Convention of Electrical and Electronics Engineers (EEIS '96)*, pp. 387–390, Jerusalem, Israel, November 1996.

[23] J. L. Barron and D. J. Fleet, "Performance of optical flow techniques," *International Journal of Computer Vision*, vol. 12, no. 1, pp. 43–77, 1994.

[24] S. Baker and I. Matthews, "Lucas-Kanade 20 years on: a unifying framework," *International Journal of Computer Vision*, vol. 56, no. 3, pp. 221–255, 2004.

[25] W. Duch and N. Jankowski, "Transfer function : hidden possibilities for better neural networks," in *Proceedings of the 16th European Symposium on Artificcial Neural Networks Bruges (ESANN '01)*, pp. 81–94, Bruges, Belgium, April 2001.